Communications on Pure and Applied Analysis
Vol. 22, No. 1, January 2023, pp. 19–39
doi:10.3934/cpaa.2021093

DATA-DRIVEN OPTIMAL CONTROL OF A SEIR MODEL FOR COVID-19

Hailiang Liu[*1] and Xuping Tian[2]

Department of Mathematics, Iowa State University
Ames, IA 50011, USA

Abstract. We present a data-driven optimal control approach which integrates the reported partial data with the epidemic dynamics for COVID-19. We use a basic Susceptible-Exposed-Infectious-Recovered (SEIR) model, the model parameters are time-varying and learned from the data. This approach serves to forecast the evolution of the outbreak over a relatively short time period and provide scheduled controls of the epidemic. We provide efficient numerical algorithms based on a generalized Pontryagin's Maximum Principle associated with the optimal control theory. Numerical experiments demonstrate the effective performance of the proposed model and its numerical approximations.

1. **Introduction.** The outbreak of COVID-19 epidemic has resulted in over millions of confirmed and death cases, evoking fear locally and internationally. It has a huge impact on global economy as well as everyone's daily life. Numerous mathematical models are being produced to forecast the spread of COVID-19 in the US and worldwide [3, 22, 9, 43]. These predictions have far-reaching consequences regarding how quickly and how strongly governments move to curb the epidemic. We aim to exploit the abundance of available data and integrate existing data with disease dynamics based on epidemiological knowledge.

Compartmental transmission models have become an invaluable tool to study the dynamics of infectious diseases. One of the well-known such models in epidemiology is the SIR model proposed by Kermack and McKendrick [36] in 1927. Here, S, I, R represent the number of susceptible, infected and recovered people respectively. They use an ODE system to describe the transmission dynamics of infectious diseases among the population. In the current COVID-19 pandemic, actions such as travel restrictions, physical distancing and self-quarantine are taken to slow down the spread of the epidemic. Typically, there is a significant incubation period during which individuals have been infected but are not yet infectious themselves. During this period the individual is in compartment E (for exposed), the resulting models are of SEIR or SEIRS type, respectively, depending on whether the acquired immunity is permanent or otherwise. Also such models can show how different public

2020 *Mathematics Subject Classification.* Primary: 34H05, 92D30; Secondary: 49M05, 49M25.
Key words and phrases. COVID-19, optimal control, epidemic model, Pontryagin's Maximum Principle, data-driven.
This research was supported by the National Science Foundation under Grant DMS1812666.
* Corresponding author.

health interventions may affect the outcome of the epidemic, and can also predict future growth patterns.

The SEIR model was shown to fit historical death record data from the 1918 Influenza epidemic [10], during which governments implemented extensive social distancing measures, including bans on public events, school closures, and quarantine and isolating measures. For the current pandemic, such model is well-suited to isolating key features and to developing policy-relevant insights. The SEIR model can certainly be further refined by including additional compartments [5].

Optimal control provides a perspective to study and understand the underlying transmission dynamics. The classical theory of optimal control was originally developed to deal with systems of controlled ordinary differential equations [26, 11]. Computational methods have been designed to solve related control problems [39, 17, 54]. There is a wide application to various fields, including those for epidemic models, with major control measures on medicine (vaccination), see e.g., [32, 7], and for Cancer immunotherapy control [14].

In this paper, we integrate the optimal control with a specific SEIR model, though the developed methods can be readily adapted to other epidemic ODE models. More precisely, we introduce a dynamic control model for monitoring the virus propagation. Here the goal is to advance our understanding of virus propagation by learning the model parameters so that the error between the reported cases and the solution to the SEIR model is minimized. In short, we formulate the following optimization problem

$$\begin{aligned} \min_{\theta} \quad & J = \sum_{i=1}^{n-1} L(U(t_i)) + g(U(T)), \\ \text{s.t.} \quad & \dot{U} = F(U,\theta) \quad t \in (0,T], \quad U(0) = U_0, \quad \theta \in \Theta. \end{aligned}$$

Here $\dot{U} = \frac{d}{dt}U(t)$, θ is a time-varying vector of model parameters, Θ is the admissible set for model parameters θ, and $U = [S, E, I, R, D]^\top$ corresponds to the susceptible, exposed, infected, recovered and deceased population. The loss function J is composed of two parts: L measures the error between the candidate solution to the SEIR system and the reported data at intermediate observation times, and g measures the error between the candidate solution and the scheduled control data at the end time.

For complicated dynamics such as the spreading of coronavirus, even the most sophisticated ODE model may not capture the true dynamics perfectly. On the other hand, if a learning algorithm is exploited to learn the parameters purely from the data without the guidance of physics, then the performance will highly depend on the reliability of the data. In contrast to conventional model predictions with standard data fitting [3, 22, 9], our data-driven optimal control algorithm provides an optimal fitting to both the data and the SEIR model.

1.1. **Main contributions.** In the present work we provide a fairly complete modeling discussion on parameter learning, prediction and control of epidemics spread based on the SEIR model. We begin with our discussion of basic properties of the SEIR model. Then we show how the parameters can be updated recursively by gradient-based methods for a short time period while parameters are near constants, where the loss gradient can be obtained by using both state and co-state dynamics. For an extended time period with reported data available at intermediate observation times, the parameters are typically time-varying. In this general setting, we

derive necessary conditions to achieve optimal control in terms of the chosen objectives. The conditions are essentially the classical Pontryagin maximum principal (PMP)[50]. The main differences are in the way we apply the principle in each time interval, and connect them consistently by re-setting the co-state V at the end of each time interval. We thus named it the generalized PMP. We further present an algorithm to find the numerical solution to the generalized PMP in the spirit of the method of successive approximations (MSA)[17]. Our algorithm is mainly fulfilled by three parts: (1) discretization of the forward problem in such a way that solutions to U remain positive for an arbitrarily step size h; (2) discretization of the co-state equation for V is made unconditionally stable; (3) Minimiziation of the Hamiltonian is given explicitly based on the structure of the SEIR model.

This data-driven optimal control approach can be applied to other epidemic models. In particular, the prediction and control can be combined into one framework. To this end, the cost includes terms measuring the error between confirmed cases (infection and death) and those predicted from the model during the evolution, and terms measuring the error between the scheduled numbers as desired and those predicted from the model during the control period.

1.2. **Further related work.** In the mathematical study of SIR models, there is an interplay between the dynamics of the disease and that of the total population, see [4, 48, 24, 56]. We refer the reader to [45, 23] for references on SEIRS models with constant total population and to [42] for the proof of the global stability of a unique endemic equilibrium of a SEIR model. Global stability of the endemic equilibrium for the SEIR model with non-constant population is more subtle, see [41]. Apart from the compartmental models (and their stochastic counterparts [2]), a wide variety of methods exist for modeling infectious disease. These include diffusion models [13], mean-field-type models [37], cellular automata [58], agent-based models [30], network-based models [57, 34, 49], and game-theoretical modelling [6, 52, 15]. Some focus on the aggregate behaviour of the compartments of the population, whereas others focus on individual behaviour.

For COVID-19, a data-driven model has been proposed and simulated in [47], where both the SIR model and the feed-forward network are trained jointly. Compared to this work, our data-driven model is to consider the optimal control for SEIR with rigorous derivation of optimality conditions and stable numerical approximations. On the other hand, our data-driven optimal control algorithm may be interpreted as training a deep neural network in which the SEIR model serves as the neural network with parameters to be learned. This is in contrast to the study of residual neural networks using neural ODEs (see e.g., [21, 16]) or section dynamics [44]. For other works on data-driven learning model parameters using neural networks, see [5, 33]. SIR models with spatial effects have been studied [8, 40]. A SIRT model was proposed in [8] to study the effects of the presence of a road on the spatial propagation of the COVID-19. Introduced in [40] is a mean-field game algorithm for a spatial SIR model in controlling propagation of epidemics.

Finally, we would like to mention that a variety of works have sought to endow neural networks with physics-motivated equations, which can improve machine learning. To incorporate the equations, parametric approaches have been studied [25, 18, 46, 51], where certain terms in the equations are learned, while the equations still govern the dynamics from input to output.

1.3. **Organization.** In Section 2, we motivate and present the SEIR system for modelling the time evolution of epidemics, and integrate it with data into an optimal control system. Both algorithms and related numerical approximations are detailed in Section 3. Section 4 provides experimental results to show the performance of our data-driven optimal control algorithms. We end with concluding remarks in Section 5.

2. The SEIR model and optimal control.

2.1. **Model formulation.** A population of size $N(t)$ is partitioned into subclasses of individuals who are susceptible, exposed (infected but not yet infectious), infectious, and recovered, with sizes denoted by $S(t), E(t), I(t), R(t)$, respectively. The sum $E + I$ is the total infected population.

The dynamical transfer of the population is governed by an ODE system

$$\begin{aligned}
\dot{S} &= A - \beta SI/N - dS,\\
\dot{E} &= \beta SI/N - \epsilon E - dE,\\
\dot{I} &= \epsilon E - \mu I - \gamma I - dI,\\
\dot{R} &= \gamma I - dR,\\
\dot{D} &= \mu I,
\end{aligned}$$

subject to initial conditions S_0, E_0, I_0, R_0, D_0. Here $D(t)$ denotes deaths at time t, A denotes the recruitment rate of the population due to birth and immigration. It is assumed that all newborns are susceptible and vertical transmission can be neglected. d is the natural death rate, μ is the rate for virus-related death. γ is the rate for recovery with $1/\gamma$ being the mean infectious period, and ϵ is the rate at which the exposed individuals become infectious with $1/\epsilon$ being the mean incubation period. The recovered individuals are assumed to acquire permanent immunity (yet to be further confirmed for COVID-19); there is no transfer from the R class back to the S class. β is the effective contact rate. Note that the involved parameters do not correspond to the actual per day recovery and mortality rates as the new cases of recovered and deaths come from infected cases several days back in time. However, one can attempt to provide some coarse estimations of the "effective/apparent" values of these epidemiological parameters based on the reported confirmed cases.

2.2. **Solution properties of the SEIR model.** Classical disease transmission models typically have at most one endemic equilibrium. If there is no endemic equilibrium, diseases will disappear. Otherwise, the disease will be persistent irrespective of initial positions. Large outbreaks tend to the persistence of an endemic state and small outbreaks tend to the extinction of the diseases.

To understand solution properties of the SEIR system, we simply take $A = bN$ with b the natural birth rate, and focus on the following sub-system

$$\begin{aligned}
\dot{S} &= bN - \beta SI/N - dS,\\
\dot{E} &= \beta SI/N - \epsilon E - dE,\\
\dot{I} &= \epsilon E - \mu I - \gamma I - dI,\\
\dot{R} &= \gamma I - dR
\end{aligned}$$

with the total population size $N = S + E + I + R$. By adding the equations above we obtain

$$\dot{N} = (b - d)N - \mu I.$$

Typically there are two time scales involved: the time of occurrence of the peak, and the entire time-span of the epidemic. Both depend on the involved model parameters. A distinct property featured by the above system is that it remains unchanged under a same scaling for all involved sub-populations. To facilitate analysis of this system, we may rewrite it in terms of population fractions. Let $s = S/N, e = E/N, i = I/N, r = R/N$ denote the fractions of the classes S, E, I, R in the population, respectively, then one can verify that

$$\dot{s} = b - bs - \beta is + \mu is, \tag{2.1a}$$

$$\dot{e} = \beta is - (\epsilon + b)e + \mu ie, \tag{2.1b}$$

$$\dot{i} = \epsilon e - (\mu + \gamma + b)i + \mu i^2, \tag{2.1c}$$

where r can be obtained from $r = 1 - s - e - i$ or

$$\dot{r} = \gamma i - br + \mu ir.$$

From biological considerations, we study system (2.1) in a feasible region

$$\Sigma = \{(s, e, i) \in \mathbb{R}^3_+, 0 \le s + e + i \le 1\}.$$

It can be verified that Σ is positively invariant with respect to the underlying dynamic system. We denote $\partial\Sigma$ and Σ^0 the boundary and the interior of Σ in $\mathbb{R}^3$, respectively. A special solution of form $P^0 = (1, 0, 0)$ on the boundary of Σ is the disease-free equilibrium of system (2.1) and it exists for all non-negative values of its parameters. Any equilibrium in the interior Σ^0 of Σ corresponds to the disease being endemic and is named an endemic equilibrium.

The following theorem, a standard type in mathematical epidemiology, shows that the basic number σ determines the long-term outcome of the epidemic outbreak (more details can be found in the appendix).

Theorem 2.1. *Let*

$$\sigma := \frac{\beta\epsilon}{(\epsilon + b)(\gamma + \mu + b)}.$$

1. *If $\sigma \le 1$, then P^0 is the unique equilibrium and globally stable in Σ.*
2. *If $\sigma > 1$, then P^0 is unstable and the system is uniformly persistent in Σ^0.*

By this theorem, the disease-free equilibrium P^0 is globally stable in Σ if and only if $\sigma \le 1$. Its epidemiological implication is that the infected fraction of the population vanishes in time so the disease dies out. In addition, the number σ serves as a sharp threshold parameter; if $\sigma > 1$, the disease remains endemic.

In the epidemic literature, another threshold quantity is the basic reproduction number

$$R_0 = \frac{\beta}{\gamma + \mu},$$

which is the product of the contact rate β and the average infectious period $\frac{1}{\gamma+\mu}$. It is a parameter well known for quantifying the epidemic spread [20, 19]. On the other hand, the contact number σ is defined at all times. In general, we have

$$R_0 \ge \sigma.$$

Note that for most models, $\sigma = R_0$, both quantities can be used interchangeably. This is the case in our experiments when taking $b = 0$.

Remark 1. Extensive evidence shows that the disease spread rate is sensitive to at least three factors: (1) daily interactions, (2) probability of infection, and (3) duration of illness. The above assertion shows that making efforts to decrease R_0 is essential for controlling propagation of epidemics. Hence measures such as social distancing (self-quarantine, physical separation), washing hands and wearing face coverings, as well as testing / timely-hospitalization can collectively decrease R_0.

Remark 2. The above model if further simplified will reduce to the SIR model or SIS model, which is easier to analyze [27, 12, 31]. It can also be enriched by dividing into different groups [38, 55], or by considering the spatial movement effects [29, 35]. In this work, we use the SEIR model as a base for our analysis, prediction, and control.

2.3. **A simple control.** In compact form, the SEIR system may be written as

$$\dot{U} = F(U;\theta), \quad U(0) = U_0,$$

where

$$U = [S, E, I, R, D]^\top, \quad \theta = [\beta, \epsilon, \gamma, \mu]^\top$$

are the column vectors of the state and parameters, respectively. Let $g(\cdot)$ be a loss function (to be specified later) at the final time T, then the problem of determining the model parameters based on this final cost can be cast as a dynamic control problem:

$$\min_\theta\{g(U(T)) \quad \text{subject to} \quad \dot{U} = F(U,\theta), \quad 0 < t \le T; \quad U(0) = U_0; \quad \theta \in \Theta\}.$$

Here the dependence of g on θ is through $U(T)$. The set of admissible parameters Θ may be estimated from other sources.

For a short time period, the model parameters are near constant, then we can use gradient-based methods to directly update θ, for which $\nabla_\theta g$ needs to be evaluated. We define the Lagrangian functional

$$\mathcal{L}(\theta) = g(U(T)) - \int_0^T (\dot{U} - F(U,\theta))^\top V dt,$$

where $V = V(t)$ is the Lagrangian multiplier depending on time and can be chosen freely, and U depends on θ through the ODE. A formal calculation gives

$$\begin{aligned}
\nabla_\theta g &= \nabla_\theta \mathcal{L} \\
&= (\nabla_\theta U(T))^\top \nabla_U g + \int_0^T \Big((\nabla_U F)(\nabla_\theta U(t)) + \nabla_\theta F - \nabla_\theta \dot{U}(t)\Big)^\top V(t) dt \\
&= (\nabla_\theta U(T))^\top (\nabla_U g - V(T)) + (\nabla_\theta U(0))^\top V(0) \\
&\quad + \int_0^T (\nabla_\theta U(t))^\top \Big((\nabla_U F)^\top V(t) + \dot{V}(t)\Big) + (\nabla_\theta F)^\top V(t) dt.
\end{aligned}$$

Thus $\nabla_\theta g$ can be determined in the following steps:

- Solve the forward problem for state U,

$$\dot{U}(t) = F(U(t),\theta), \quad U(0) = U_0.$$

- Solve the backward problem for co-state V,

$$\dot{V}(t) = -(\nabla_U F)^\top V(t), \quad V(T) = \nabla_U g(U(T)).$$

- Evaluate the gradient of g by

$$\nabla_\theta g = \int_0^T (\nabla_\theta F)^\top V(t)dt.$$

Note that the optimality condition is that the gradient needs to vanish when the minimizer is strictly within $\theta \in \Theta$, while the (U, V) dynamical system models the optimal strategies for S, E, I, R populations.

Remark 3. In the context of the optimal control theory, such V exists and is called the co-state function. The above relations are essentially derivable from the classical PMP optimality conditions [50].

2.4. **Data-driven optimal control.** Now we consider an extended time period with reported data available at intermediate observation times. The data are taken from the reported cumulative infection and death cases.[1] In such general case the parameters are typically time-varying, we need to derive a more refined data-driven optimal control. Arranging the data in a vector $U_c = [I_c, D_c]^\top$ at times $0 = t_0 < t_1 < t_2 < ... < t_n = T$, we aim to

- find optimal parameter $\theta(t)$ for $0 \le t \le t_{n-1}$ such that the solution to the SEIR system fits the reported data at the grid points $\{t_i\}_{i=1}^{n-1}$ as close as possible, and
- find desired parameter $\theta(t)$ for $t_{n-1} \le t \le T$ that is able to control the epidemic spreading at time T at desired values.

To achieve these goals, we first define a loss function by

$$J = \sum_{i=1}^{n-1} L(U(t_i)) + g(U(T)),$$

where

$$\begin{aligned} L(U(t_i)) &= \lambda_1 |I(t_i) - I_c(t_i)|^2 + \lambda_2 |D(t_i) - D_c(t_i)|^2, \quad 1 \le i \le n-1, \\ g(U(T)) &= \lambda_1 |I(T) - I_d(T)|^2 + \lambda_2 |D(T) - D_d(T)|^2. \end{aligned} \tag{2.2}$$

Here λ_1, λ_2 are user-defined normalization factors. In our experiments, λ_1, λ_2 are chosen such that the loss with respect to the infection cases is at the same level of scales as the loss with respect to the death cases. This loss function is composed of two parts: the running cost L which measures the error between the candidate solution (I, D) to the SEIR system and the reported data (I_c, D_c) at intermediate times; and the final cost g, which measures the error between the candidate solution (I, D) and the desired data (I_d, D_d) at the end time.

We then formulate the task as the following optimal control problem

$$\begin{aligned} \min \quad & J = \sum_{i=1}^{n-1} L(U(t_i)) + g(U(T)), \\ \text{s.t.} \quad & \dot{U} = F(U, \theta) \quad t \in (0, T], \quad U(0) = U_0, \quad \theta \in \Theta. \end{aligned} \tag{2.3}$$

Motivated by the classical optimal control theory, we derive the necessary conditions for the optimal solution to problem (2.3), stated in the following theorem.

[1] Data used here is publicly available in the CSSEGISandData/COVID-19 GitHub repository, which collects data from official sources and organizations.

Theorem 2.2. *Let θ^* be the optimal solution to problem (2.3) and U^* be the corresponding state function, then there exists a piece-wise smooth function V^* and a Hamiltonian H defined by*

$$H(U,V,\theta) = V^\top F(U,\theta) \tag{2.4}$$

such that

$$\dot{U^*} = F(U^*,\theta^*), \quad t\in(0,T], \quad U^*(0)=U_0, \tag{2.5}$$

$$\begin{aligned} \dot{V^*} &= -(\nabla_U F(U^*,\theta^*))^\top V, \quad t_{i-1}\le t<t_i, \quad i=n,...,1,\\ V^*(T) &= \nabla_U g(U^*(T)), \\ V^*(t_i^-) &= V^*(t_i^+) + \nabla_U L(U^*(t_i)), \quad i=n-1,...,1 \end{aligned} \tag{2.6}$$

are satisfied. Moreover, the Hamiltonian minimization condition

$$H(U^*,V^*,\theta^*) \le H(U^*,V^*,a) \quad \forall a\in\Theta$$

holds for all time $t\in[0,T]$ but $\{t_i\}_{i=1}^{n-1}$.

Proof. Recall the classical Bolza optimal control problem [11]

$$\begin{aligned} \min \quad & \left\{ \int_0^T L(U(t),\theta(t))dt + g(U(T)) \right\} \\ \text{s.t.} \quad & \dot{U} = F(U,\theta), \quad t\in[0,T], \quad U(0)=U_0, \quad \theta(t)\in\Theta. \end{aligned}$$

The Pontryagin's maximum principle states the necessary conditions for optimality: assume θ^* and U^* are the optimal control function and corresponding state of the system, then there exists a function V^* and a Hamiltonian H defined for all $t\in[0,T]$ by

$$H(U,V,\theta) = V^T F(U,\theta) + L(U,\theta)$$

such that

$$\dot{U^*} = \nabla_V H(U^*,V^*,\theta^*), \quad U^*(0)=U_0, \tag{2.7}$$

$$\dot{V^*} = -\nabla_U H(U^*,V^*,\theta^*), \quad V^*(T) = \nabla_U g(U^*(T)), \tag{2.8}$$

are satisfied. Moreover, the Hamiltonian minimization condition

$$H(U^*,V^*,\theta^*) \le H(U^*,V^*,a)$$

holds for all time $t\in[0,T]$ and for all permissible control function $a\in\Theta$.

Notice that the loss function in (2.3) can be approximated by

$$J_\epsilon = \int_0^T \sum_{i=1}^{n-1} L(U(t))\eta_\epsilon(t-t_i)dt + g(U(T)).$$

Here η_ϵ is a mollifier function defined by

$$\eta_\epsilon(t-t_i) = \frac{1}{\epsilon}\eta\left(\frac{t-t_i}{\epsilon}\right), \tag{2.9}$$

where $\epsilon \le \frac{1}{2}\min_{0\le i\le n-1}|t_{i+1}-t_i|$ is kept fixed. This η_ϵ is supported on $[-1,1]$ and sufficient smooth with integral one. Now the corresponding Hamiltonian reads as

$$H(U,V,\theta) = V^T F(U,\theta) + \sum_{i=1}^{n-1} L(U(t))\eta_\epsilon(t-t_i). \tag{2.10}$$

Hence (2.7) can be expressed as (2.5), (2.8) has the form of

$$\dot{V} = -\sum_{i=1}^{n-1} \nabla_U L(U(t))\eta_\epsilon(t-t_i) - (\nabla_U F(U,\theta))^\top V, \quad V(T) = \nabla_U g(U(T)). \quad (2.11)$$

Integrate (2.11) from $t_i^- - \epsilon_1$ to $t_i^+ + \epsilon_1$ with $\epsilon_1 \le \epsilon$. Let ϵ tend to 0, then for $i = n-1, ..., 1$, we have

$$V(t_i^+) - V(t_i^-) = \nabla_U L(U(t_i)).$$

Thus in each interval, (2.11) reduces to

$$\dot{V} = -(\nabla_U F(U,\theta))^\top V, \quad t_{i-1} \le t < t_i, \quad i = n, ..., 1,$$

which is exactly (2.6). Correspondingly, the Hamiltonian (2.10) reduces to (2.4) for all $t \in [0,T]$ but $\{t_i\}_{i=1}^{n-1}$. Finally, we can identify J as the limit of J_ϵ. In fact,

$$\begin{aligned} |J_\epsilon - J| &= \left| \int_0^T \sum_{i=1}^{n} \eta_\epsilon(t-t_i)[L(U(t)) - L(U(t_i))]dt \right| \\ &\le \sum_{i=1}^{n} \max_{(t_i-\epsilon, t_i+\epsilon)} |L(U(t)) - L(U(t_i))| \to 0 \end{aligned}$$

as $\epsilon \to 0$. Here we have used the fact that $U(t)$ is continuous and the definition of L. This completes the proof. □

3. **Numerical discretization and algorithms.** In this section, we present implementation details to solve problem (2.3) via solving the generalized PMP by iteration. We proceed in the following manner. First we make an initial guess $\theta_0 \in \Theta$. From the control function $\theta_l(t)$ in the l-th iteration for $l = 0, 1, 2, \cdots$, we obtain $\theta_{l+1}(t)$ in three steps:

Step 1: Solve the forward problem (2.5) to obtain U_l.

Step 2: Solve the sequence of backward problems (2.6) to obtain V_l.

Step 3: $\theta_{l+1} = \text{argmin}_{\theta\in\Theta} H(U_l, V_l, \theta, t)$ for each $t \in [0,T]$.

This is essentially the method of successive approximations (MSA) [17]. An important feature of MSA is that the Hamiltonian minimization step is decoupled for each t. However, in general MSA tends to diverge, especially if a bad initial guess is taken [17].

Our strategy is to adopt a careful discretization at each step to control possible divergent behavior, instead of simply calling an existing ODE solver for Steps 1-2, and an optimization algorithm for Step 3.

Within each interval (t_{i-1}, t_i), we approximate both U and V at the same m points with step size $h = (t_i - t_{i-1})/m$, so that the value of U required in Step 2 are already calculated in Step 1. We use $U^{i,k}, V^{i,k}, \theta^{i,k}$, where $i = 1, ..., n$ and $k = 0, ..., m$ to denote solution values at k-th point in the i-th interval.

Note that population dynamics (births or deaths) may be neglected at a very crude level on the grounds that epidemic dynamics often occur on a faster time scale than host demography, or we can say heuristically that death of an infected individual and subsequent replacement by a susceptible (in the absence of vertical transmission) is equivalent to a recovery event. Hence, in the numerical study, both b and d are taken to be zero.

Below we discuss the discretization of the three iteration steps for the case $b = d = 0$.

3.1. **Forward discretization.** We focus on the time interval (t_{i-1}, t_i). For notation simplicity, we use U^k, V^k, θ^k to represent corresponding values at the k-th point. We discretize the forward problem (2.5) by an explicit-implicit method with the Gauss-Seidel type update:

$$\begin{aligned}
\frac{S^{k+1}-S^k}{h} &= -\beta^k S^{k+1} I^k / N^k,\\
\frac{E^{k+1}-E^k}{h} &= \beta^k S^{k+1} I^k / N^k - \epsilon^k E^{k+1},\\
\frac{I^{k+1}-I^k}{h} &= \epsilon^k E^{k+1} - (\gamma^k + \mu^k) I^{k+1},\\
\frac{R^{k+1}-R^k}{h} &= \gamma^k I^{k+1},\\
\frac{D^{k+1}-D^k}{h} &= \mu^k I^{k+1}.
\end{aligned}$$

The most important property of this update (see the explicit formula (B.1) in appendix) is its unconditional positivity-preserving property, i.e,

$$U^k \geq 0 \Rightarrow U^{k+1} > 0,\ k = 0, \cdots$$

irrespective of the size of the step size h. For the starting value in each interval, we have

$$U^{1,0} = U(0), \quad U^{i,0} = U^{i-1,m}, \quad i = 2, \cdots, n-1.$$

3.2. **Backward discretization.** Let $V = [V_S, V_E, V_I, V_R, V_D]^\top$, with the numerical solution $\{S^k, E^k, I^k, R^k, D^k\}_{k=0}^m$ to the forward equation (2.5) known, the backward equation (2.6) needs to be discretized correspondingly. In a similar fashion to the update of U, we derive the update of V with an explicit-implicit discretization by

$$\begin{aligned}
\frac{V_S^{k+1}-V_S^k}{h} &= \beta^k I^k (N^k - S^k)(V_S^k - V_E^{k+1})/(N^k)^2,\\
\frac{V_E^{k+1}-V_E^k}{h} &= \epsilon^k (V_E^k - V_I^{k+1}),\\
\frac{V_I^{k+1}-V_I^k}{h} &= \beta^k S^k (N^k - I^k)(V_S^k - V_E^k)/(N^k)^2\\
&\quad + \gamma^k (V_I^k - V_R^{k+1}) + \mu^k (V_I^k - V_D^{k+1})\\
V_R^k = V_R^{k+1}, &\quad V_D^k = V_D^{k+1}.
\end{aligned}$$

For the starting value in each interval, we have

$$V^{n,m} = \nabla_U g(U(T)), \quad V^{i,m} = V^{i+1,0} + \nabla_U L(U(t_i)), \quad i = n-1, \cdots, 1.$$

Note that the above discretization is well-defined for any $h > 0$ (see details and the explicit formula (B.2) in appendix), hence unconditionally stable since the system is linear in V.

3.3. **Hamiltonian minimization.** The Hamiltonian (2.4) is given by

$$\begin{aligned}
H(U, V, \theta) = &-V_S \beta S I/N + V_E(\beta S I/N - \epsilon E)\\
&+ V_I(\epsilon E - (\gamma + \mu) I) + V_R \gamma I + V_D \mu I.
\end{aligned}$$

After plugging in $U(t), V(t)$ that is obtained by solving the above forward and backward problems with given $\theta(t)$, H may be seen as a functional only with respect

to θ. We solve it by the proximal point algorithm (PPA) [53], that is for any fixed time $t \in (t_{i-1}, t_i)$, $i = 1, 2, ..., n$,

$$\theta_{l+1}(t) = \text{argmin}_{\theta(t)\in\Theta} \left\{ H(U_l(t), V_l(t), \theta(t)) + \frac{1}{2\tau}\|\theta(t) - \theta_l(t)\|^2 \right\}, \tag{3.1}$$

where l is the index for iteration, τ is the step size.

Remark 4. The use of PPA brings two benefits: (1) the objective function in (3.1) is a convex function, which ensures the existence of the solution to the minimization problem; (2) it is numerically stable: PPA has the advantage of being monotonically decreasing, which is guaranteed for any step size $\tau > 0$. In this way, the convergence of minimizing the original loss in (2.3) with a regularization term is ensured, hence address the convergence issue that MSA generally has [1].

Given discretized U^α and V^α with $\alpha = \{i, k\}$, we solve (3.1) on grid points, that is to solve

$$\theta^\alpha_{l+1} = \text{argmin}_{\theta\in\Theta} \left\{ H(U^\alpha_l, V^\alpha_l, \theta) + \frac{1}{2\tau}\|\theta - \theta^\alpha_l\|^2 \right\}. \tag{3.2}$$

Since H is smooth, the above formulation when the constraint is not imposed is equivalent to the following

$$\theta^\alpha_{l+1} = \theta^\alpha_l - \tau\nabla_\theta H(U^\alpha_l, V^\alpha_l, \theta^\alpha_{l+1}).$$

The special form of H allows us to obtain a closed form solution:

$$\begin{aligned}
\beta^\alpha_{l+1} &= \beta^\alpha_l + \tau S^\alpha_l I^\alpha_l((V_S)^\alpha_l - (V_E)^\alpha_l)/N^\alpha_l,\\
\epsilon^\alpha_{l+1} &= \epsilon^\alpha_l + \tau E^\alpha_l((V_E)^\alpha_l - (V_I)^\alpha_l),\\
\gamma^\alpha_{l+1} &= \gamma^\alpha_l + \tau I^\alpha_l((V_I)^\alpha_l - (V_R)^\alpha_l),\\
\mu^\alpha_{l+1} &= \mu^\alpha_l + \tau I^\alpha_l((V_I)^\alpha_l - (V_D)^\alpha_l).
\end{aligned} \tag{3.3}$$

Now taking the constraint $\theta \in \Theta$ into consideration, we simply project the solution (3.3) back into the feasible region after each iteration, that is

$$\theta^\alpha_{l+1} = \text{clip}(\theta^\alpha_{l+1}, \underline{\Theta}, \overline{\Theta})$$

where $\underline{\Theta}$, $\overline{\Theta}$ are element-wise lower bound and upper bound of Θ, respectively. That guarantees the output is constrained to be in Θ.

Remark 5. The step size for each parameter may be set differently according to their magnitude scale, and this can indeed improve the training performance, as observed in our experiments. The above clip$(\cdot)$ function is simply a projection on the box constraints. For a general convex set Θ, a more refined limiter is needed to pull the parameters back to the feasible region.

3.4. **Algorithms.** The above computing process is wrapped up in Algorithm 1. Since we can update $\{\theta^{i,k}\}$ simultaneously, we consider $\{\theta^{i,k}\}$ as a vector and still denote it as θ for notational simplicity. We use $\|\cdot\|$ to stand for the L_2 norm.

Initialization: We now discuss how to initialize the control function θ. A simple choice is to take $\theta^{i,k}_0$ to be a constant vector for all $1 \le i \le n, 1 \le k \le m$, where the value of each component relies on a priori epidemiological and clinical information about the relative parameter magnitude. They vary with the area from where the data were sampled.

Algorithm 1

Require: $\{U_c(t_i)\}_{i=1}^n$: data, $t_n = T$: final time, U_0: initial data at 0, θ_0: initial guess, τ: step size for the minimization problem

while $\|\theta_l - \theta_{l-1}\|/\|\theta_{l-1}\| >$ Tol **do**
  for $i = 1$ to n **do**
    for $k = 0$ to $m-1$ **do**
      $U^{i,k+1} \leftarrow U^{i,k}$ (solve the forward problem, refer to (B.1))
    $U^{i,0} \leftarrow U^{i-1,m}$ (update the initial condition for ODE solver)
  $V^{n,m} \leftarrow \partial_U g(U(T))$ (set the initial data for the backward problem)
  for $i = n$ to 1 **do**
    for $k = m-1$ to 0 **do**
      $V^{i,k} \leftarrow V^{i,k+1}$ (solve the backward problem, refer to (B.2))
    $V^{i,m} \leftarrow V^{i+1,0} + \partial_U L(U(t_i))$ (update the initial condition for ODE solver)
  $\theta_{l+1} \leftarrow \theta_l$ (solve the minimization problem, refer to (3.3))
  $\theta_{l+1} \leftarrow \text{clip}(\theta_{l+1}, \underline{\Theta}, \overline{\Theta})$ (ensure $\theta \in \Theta$)
return θ, U

We can also use the data $\{D_c(t_i)\}_{i=0}^n, \{I_c(t_i)\}_{i=0}^n$ to obtain a better initial guess for μ. More precisely, from $\mu = \dot{D}/I$ we take

$$\mu_0^{i,k} = \frac{D_c(t_{i+1}) - D_c(t_i)}{(t_{i+1} - t_i) I_c(t_{i+1})} \quad \forall k = 0, 1, ..., m.$$

The initial data for the forward problem is set as

$$U_0 = [N(0) - I_c(0), 0, I_c(0), 0, D_c(0)]^\top,$$

where $N(0)$ is the initial population of the area analyzed, $I_c(0)$, $D_c(0)$ are the confirmed infections and deaths on the day of the first confirmed cases, respectively.

The initial condition of the backward problem is given in (2.6). In the present setup, the loss function g only depends on I and D, hence the initial condition is given by

$$V^{n,m} = [0, 0, \partial_I g(U(T)), 0, \partial_D g(U(T))]^\top.$$

Finally, we should point out that Algorithm 1 with a rough initial guess θ_0 can be rather inefficient when T is large. In such case, we divide the whole interval as $0 = t_{n_0} < t_{n_1} < ... < t_{n_s} < t_{n_{s+1}} = T$ with $t_{n_j} \in \{t_i\}_{i=1}^{n-1}$ for $1 \le j \le s$ and apply Algorithm 1 to each subinterval consecutively. This treatment is summarized in Algorithm 2.

Algorithm 2

Require: $\{U_c(t_i)\}_{i=1}^n$, U_0: initial data, τ: step size for the minimization problem.
Require: $\{t_{n_j}\}_{j=0}^{s+1}$, θ_0: initial guess of θ on $[t_{n_0}, t_{n_1}]$

for $j = 0$ to s **do**
  $\theta, U =$ Algorithm 1($\{U_c(t_i)\}_{i=n_j+1}^{n_{j+1}}$, $[t_{n_j}, t_{n_{j+1}}]$, U_0, θ_0, τ)
  $\theta_0, U_0 \leftarrow \theta(t_{n_{j+1}}), U(t_{n_{j+1}})$
  return θ, U

Remark 6. (i) If parameters vary dramatically, $\theta(t_{n_j})$ may not be a good initialization for θ on $[t_{n_j}, t_{n_{j+1}}]$. When this happens we switch to the rough initial guess and test by trial and error.

(ii) With Algorithm 2, we can easily fit the data in a large period of time by simply dividing it into several subintervals, then applying Algorithm 1 in each subinterval. They can even be trained simultaneously as long as we have initial data for each subinterval. However, in the COVID-19 case, only partial data (infection cases and death cases) are available. We dont have access to the full initial data for the SEIR model except in the very beginning. This is why we train the model consecutively since the solution in the previous subinterval gives the initial data to the next subinterval.

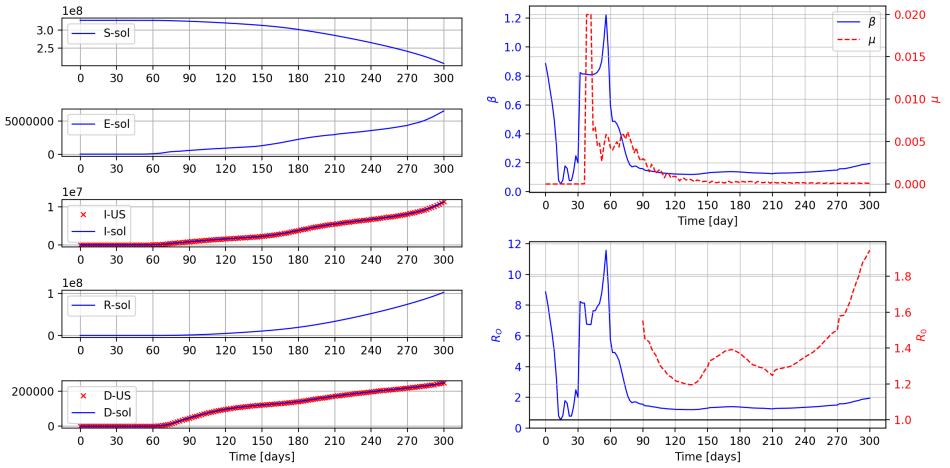

(a) (b)

FIGURE 1. (a) Reported and fitted cumulative infection and death cases in the US (b) Estimated SEIR parameters and the basic reproduction number. β (μ) corresponds to the left (right) vertical axis, $\epsilon = 0.2$ and $\gamma = 0.1$ are almost constant. The dashed line in R_0 is a zoomed-in version on the tail of the solid line.

4. **Experiments.** We now present experimental results to demonstrate the good performance of our algorithms.[2] In all the experiments, the normalization factors λ_1, λ_2 in (2.2) are chosen such that the loss with respect to the infection cases is at the same scale as the loss with respect to the death cases. According to the Centers for Disease Control and Prevention (CDC) in the US, the median incubation period is 4-5 days from exposure to symptoms onset, persons with mild to moderate COVID-19 remain infectious no longer than 10 days after symptom onset, therefore, we set

$$\Theta = \{\theta \,|\, 0 \le \beta \le 5,\ 0.2 \le \epsilon \le 0.25,\ 0.1 \le \gamma \le 0.2,\ 0 \le \mu \le 0.01\}.$$

[2]We make our code available at https://github.com/txping/op-seir

For the step size, considering that β, ϵ and γ are almost at the same scale, which is 100 times greater than μ, and the permissible range of β is much large than ϵ and γ, we set $\tau_\epsilon = \tau_\gamma = \tau$, $\tau_\beta = 100\tau$ and $\tau_\mu = \tau/100$.

4.1. **Covid-19 epidemic in the US.** As of today [November 17, 2020], it has been about 300 days since the first infection case of COVID-19 was reported in the US. We thus consider the time period $[0, 300]$ and sample the data $[I_c, D_c]$ at $t_i = 2i$ for $0 < i \leq 150$. To apply Algorithm 2 we take $\{t_{n_j}\}_{j=0}^{s+1}$ as {0, 30, 60, 90, 150, 210, 270, 300}.

Data fitting via optimal control with SEIR model. Figure 1 (a) shows that our data-driven optimal control algorithm learns the data very well. In Figure 1 (b), there is a noticeable peak over the second month, where the value of reproduction number R_0 is very large due to a dramatic increase in infection rate β. After that, R_0 goes down to a lower range, with a slight rise around the 6-th month. Over the last two months we observed another increase in R_0. Overall, the value of R_0 stays above 1 and the pattern of R_0 is consistent with the increasing trend of the confirmed cases. For a short time period, one may expect the transmission to continue the same way, then the learned model parameters could be used for prediction over a short coming period.

Remark 7. We note that there are advanced machine learning methods such as the long short-term memory model [28] to predict θ in the forecasting window, which could potentially boost the prediction accuracy.

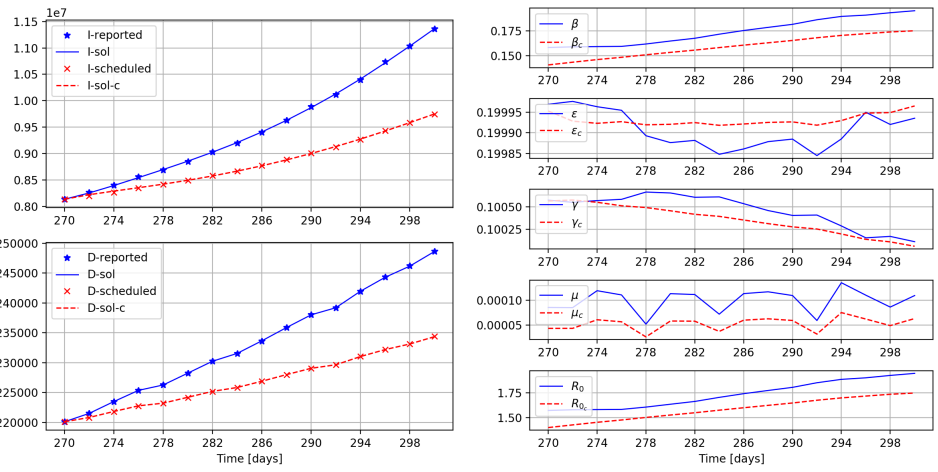

(a) (b)

FIGURE 2. Scheduled control for the US in 270 − 300 days by SEIR model

Scheduled control. From the above prediction result, we see that without interventions, the amount of confirmed and death cases will increase rapidly. We would like to see a slow down of the epidemic spreading as the outcome of various public health interventions. With the present approach, this can be formulated as a scheduled control. Specifically, with a target level of infection and death cases at

the final time T, we schedule a sequence of values at intermediate times, from which we apply our algorithm to learn the optimal parameters (control function) such that the state function reaches the desired value at T along the scheduled path.

For instance, starting from the 270-th day, with the goal of controlling the cumulative number of infection and death cases at $9,746,063$ and $234,390$ on the 300-th day, respectively, we set a pair of values for each day in the 30 days as shown in Figure 2 (a), then learn the parameters from the scheduled data. The results are presented in 2 (b). Figure 2 (a) shows that the goal can be achieved by setting the parameters as what have been learned.

To compare the situations with or without a scheduled control, we also present the reported data and corresponding training results in Figure 2. In fact, the scheduled intermediate values are obtained by assuming the daily increases were half of the reported daily increases. From Figure 2 (b), we see that the most significant difference occurs in β. This can be roughly interpreted as: if the contact rate β could be reduced by 0.02, the number of confirmed cases over the last 30 days could have been reduced by 50%, though the corresponding R_0 is still greater than 1. For virus propagation to eventually stop, R_0 needs to be less than 1, for which β must be less than $\gamma + \mu$.

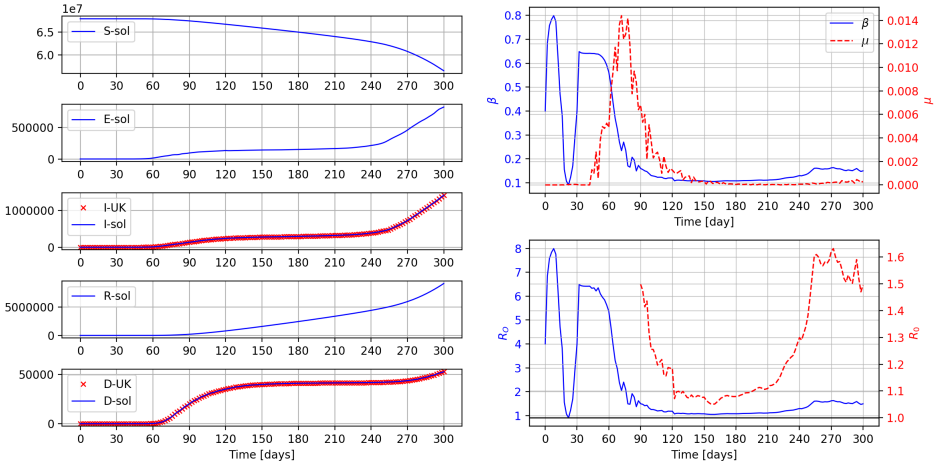

(a) (b)

FIGURE 3. (a) Reported and fitted cumulative infection and death cases in the UK (b) Estimated SEIR parameters and the basic reproduction number. β (μ) corresponds to the left (right) vertical axis, $\epsilon = 0.2$ and $\gamma = 0.1$ are almost constant. The dashed line in R_0 is a zoomed-in version on the tail of the solid line.

4.2. **Experimental results for other countries.** The coronavirus pandemic continues to affect every region of the world, but some countries are experiencing higher rates of infection, while others appear to have mostly controlled the virus. In order to see the virus dynamics in other regions, we also provide results for some other selected countries such as the UK, France and China. For the UK, $\{t_{n_j}\}_{j=0}^{s+1}$ are taken as $\{0, 30, 90, 120, 150, 180, 210, 240, 300\}$. For France, $\{t_{n_j}\}_{j=0}^{s+1}$ are taken

as $\{0, 30, 60, 90, 180, 300\}$. For China, $\{t_{n_j}\}_{j=0}^{s+1}$ are taken as $\{0, 30, 60, 90, 120, 150, 180, 210, 240, 270, 300\}$.

From Figure 3 and 4, we see that the confirmed cases in UK and France display similar patterns. Figure 5 shows that China was hit hard early on, but the number of new cases has largely been under control for months.

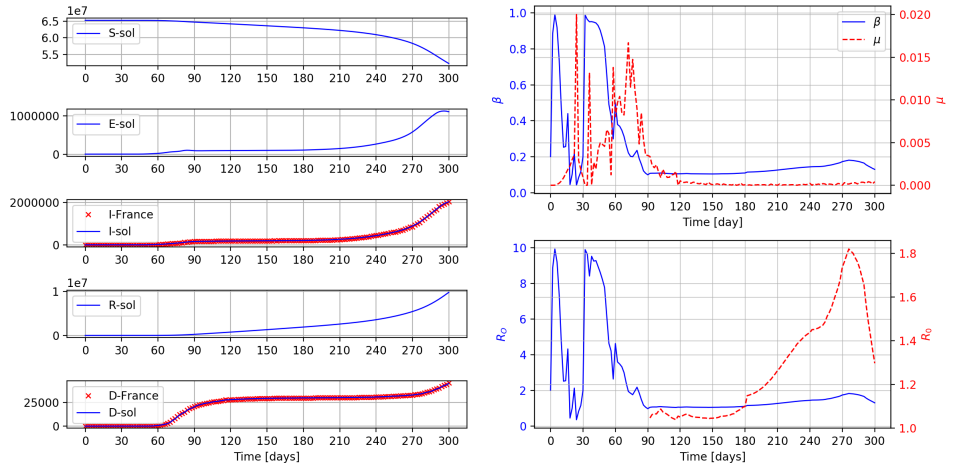

(a) (b)

FIGURE 4. (a) Reported and fitted cumulative infection and death cases in France (b) Estimated SEIR parameters and the basic reproduction number. β (μ) corresponds to the left (right) vertical axis, $\epsilon = 0.2$ and $\gamma = 0.1$ are almost constant. The dashed line in R_0 is a zoomed-in version on the tail of the solid line.

5. **Discussion.** In this paper, we introduced a data-driven optimal control model for learning the time-varying parameters of the SEIR model, which reveals the virus spreading process among several population groups. Here the state variables represent the population status, such as S, E, I, R, D while the control variables are rate parameters of transmission among population groups. The running cost is of discrete form fitting the reported data of infection and death cases at the observation times. The terminal cost serves to quantify the desired level of the total infection and death cases at scheduled times. Numerical algorithms are derived to solve the proposed model efficiently. Experimental results show that our approach can effectively fit, predict and control the infected and deceased populations.

Our experimental results suggest that our model has the potential to quantify the overall virus transmission process accurately, especially for capturing little spikes and dips. This can be helpful when studying the effects of certain interventions or events on the virus transmission. For example, it can be observed in Figure 1 (b) that there is an obvious decrease of R_0 at the end of March, which indicates that the Stay-at-Home order is an effective measure to control the virus transmission. We also see a little spike of R_0 starting from the beginning of June [$\sim$ 135-th day]. This implies that mass gathering does speed up the spreading of virus transmission, while it has less effect on the death rate. In addition, our model allows to be incorporated

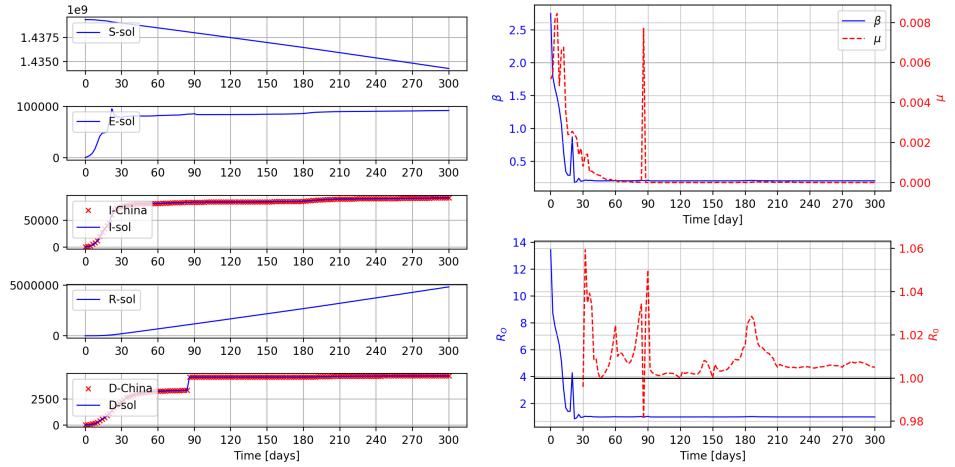

(a) (b)

FIGURE 5. (a) Reported and fitted cumulative infection and death cases in China (b) Estimated SEIR parameters and the basic reproduction number. β (μ) corresponds to the left (right) vertical axis, $\epsilon = 0.2$ and $\gamma = 0.2$ are almost constant. The dashed line in R_0 is a zoomed-in version on the tail of the solid line.

with a scheduled control strategy. This helps to reach a desired level of infection and death cases at scheduled intermediate times. In this aspect, our simulation tools can be particularly useful for policymakers to take steps to manage the public health and economic risks associated with the outbreak.

The data-driven modeling approach presented in this work is applicable to more refined models such as those including additional compartments to model vaccinated and asymptomatic individuals, and different stages of disease progression. The equations may also include multiple groups to model heterogeneity, age, spatial structure or host species. On the computational side, our approach involves a non-convex optimization problem, which comes from the multiplicative terms of the SEIR model itself. In future work, we intend to extend our algorithm to more refined models.

Appendix A. **Solution properties of the SEIR model.** To identify the critical threshold for the parameters, we take $\epsilon\times$(2.1b)$+$ $(\epsilon+b)\times$(2.1c) to obtain

$$\begin{aligned}\frac{d}{dt}[\epsilon e + (\epsilon+b)i] &= i\left[\epsilon\beta s + \epsilon\mu e + \mu(\epsilon+b)i - (\epsilon+b)(\gamma+\mu+b)\right]\\ &\le i\left[\max\{\epsilon\beta, \epsilon\mu, \mu(\epsilon+b)\} - (\epsilon+b)(\gamma+\mu+b)\right] \le 0,\end{aligned}$$

provided a key quantity $\sigma \le 1$, where

$$\sigma := \frac{\beta\epsilon}{(\epsilon+b)(\gamma+\mu+b)}$$

is called the modified contact number [41]. The global stability of P^0 when $\sigma \le 1$ follows from LaSalle's invariance principle.

Appendix B. **Numerical discretization.** Here we provide some calculation details on the forward discretization and backward discretization.

B.1. **Forward discretization.** The update scheme for solving the forward equation is given by:

$$\begin{aligned} S^{k+1} &= \frac{S^k}{1+h\beta^k I^k/N^k}, \\ E^{k+1} &= \frac{E^k + h\beta^k S^{k+1} I^k/N^k}{1+h\epsilon^k}, \\ I^{k+1} &= \frac{I^k + h\epsilon^k E^{k+1}}{1+h(\gamma^k+\mu^k)}, \\ R^{k+1} &= R^k + h\gamma^k I^{k+1}, \\ D^{k+1} &= D^k + h\mu^k I^{k+1}, \end{aligned} \tag{B.1}$$

where $k = 0, 1, ..., m-1$, $h = (t_i - t_{i-1})/m$ is the step size.

B.2. **Backward discretization.** By calculation,

$$\nabla_U F = \begin{bmatrix} -\beta I(N-S)/N^2 & 0 & -\beta S(N-I)/N^2 & 0 & 0 \\ \beta I(N-S)/N^2 & -\epsilon & \beta S(N-I)/N^2 & 0 & 0 \\ 0 & \epsilon & -(\mu+\gamma) & 0 & 0 \\ 0 & 0 & \gamma & 0 & 0 \\ 0 & 0 & \mu & 0 & 0 \end{bmatrix},$$

then (2.6) takes the following form

$$\begin{aligned} \dot{V_S} &= \beta I(N-S)(V_S - V_E)/N^2, \\ \dot{V_E} &= \epsilon(V_E - V_I), \\ \dot{V_I} &= \beta S(N-I)(V_S - V_E)/N^2 + \gamma(V_I - V_R) + \mu(V_I - V_D), \\ \dot{V_R} &= \dot{V_D} = 0. \end{aligned}$$

After discretization by the explicit-implicit method, the backward equation can be solved by the update scheme:

$$\begin{aligned} V_S^k &= \frac{V_S^{k+1}(N^k)^2 + h\beta^k I^k (N^k - S^k) V_E^{k+1}}{(N^k)^2 + h\beta^k I^k (N^k - S^k)}, \\ V_E^k &= \frac{V_E^{k+1} + h\epsilon^k V_I^{k+1}}{1+h\epsilon^k}, \\ V_I^k &= \frac{V_I^{k+1} + h\left(\gamma^k V_R + \mu^k V_D - \beta^k S^k (N^k - I^k)(V_S^k - V_E^k)/(N^k)^2\right)}{1+h(\gamma^k+\mu^k)}, \\ V_R^k &= V_R^{k+1}, \qquad V_D^k = V_D^{k+1}, \end{aligned} \tag{B.2}$$

where $k = m-1, ..., 0$, $h = (t_i - t_{i-1})/m$ is the step size.

REFERENCES

[1] V. V. Aleksandrov, On the accumulation of perturbations in the linear systems with two coordinates, *Vestnik MGU*, **3**.

[2] L. J. S. Allen, An introduction to stochastic epidemic models, in *Mathematical Epidemiology*, vol. 1945, Springer, Berlin, 2008,

[3] C. Anastassopoulou, L. Russo, A. Tsakris and C. Siettos, Data-based analysis, modelling and forecasting of the COVID-19 outbreak, *PLOS ONE*, **15** (2020), 1–21.

[4] R. M. Anderson and R. M. May, Population biology of infectious diseases: Part I, *Nature*, **280** (1979), 361–367.
[5] S. Arik, C. L. Li, J. Yoon, R. Sinha, A. Epshteyn, L. T. Le, V. Menon, S. Singh, L. Zhang, M. Nikoltchev, Y. K. Sonthalia, H. Nakhost, E. Kanal and T. Pfister, Interpretable sequence learning for covid-19 forecasting, arXiv:2008.00646.
[6] C. T. Bauch and D. J. D. Earn, Vaccination and the theory of games, *Proc. Natl. Acad. Sci. USA*, **101** (2004), 13391–13394.
[7] H. Behncke, Optimal control of deterministic epidemics, *Optim. Contr. Appl. Met.*, **21** (2000), 269–285.
[8] H. Berestycki, J. M. Roquejoffre and L. Rossi, Propagation of epidemics along lines with fast diffusion, arXiv:2005.01859.
[9] A. Bertozzi, E. Franco, G. Mohler, M. Short and D. Sledge, The challenges of modeling and forecasting the spread of COVID-19, *P. Natl. Acad. Sci.*, **117** (2020), 16732–16738.
[10] M. C. J. Bootsma and N. M. Ferguson, The effect of public health measures on the 1918 influenza pandemic in u.s. cities, *P. Natl. Acad. Sci.*, **104** (2007), 7588–7593.
[11] A. Bressan and B. Piccoli, *Introduction to the mathematical theory of control*, in AIMS Series on Applied Mathematics, American Institute of Mathematical Sciences (AIMS), Springfield, MO, 2007.
[12] F. Brauer and C. Castillo-Chávez, *Mathematical Models in Population Biology and Epidemiology*, Springer-Verlag, New York, 2001.
[13] V. Capasso, Reaction-diffusion models for the spread of a class of infectious diseases, in *Proceedings of the Second European Symposium on Mathematics in Industry (Oberwolfach, 1987)*, vol. 3 of European Consort. Math. Indust., Teubner, Stuttgart, 1988,
[14] F. Castiglione and B. Piccoli, Cancer immunotherapy, mathematical modeling and optimal control, *J. Theor. Biol.*, **247** (2007), 723–732.
[15] S. L. Chang, M. Piraveenan, P. Pattison and M. Prokopenko, Game theoretic modelling of infectious disease dynamics and intervention methods: a review, *J. Biol. Dyn.*, **14** (2020), 57–89.
[16] R. T. Q. Chen, Y. Rubanova, J. Bettencourt and D. K. Duvenaud, Neural ordinary differential equations, in *Conference on Neural Information Processing Systems (NIPS)*, 2018.
[17] F. L. Chernous and A. A. Lyubushin, Method of successive approximations for solution of optimal control problems, *Optimal Control Appl. Methods*, **3** (1982), 101–114.
[18] M. Cranmer, S. Greydanus, S. Hoyer, P. Battaglia, D. Spergel and S. Ho, Lagrangian neural networks, arXiv:2003.04630.
[19] P. van den Driessche and J. Watmough, Reproduction numbers and sub-threshold endemic equilibria for compartmental models of disease transmission, *Math. Biosci.*, **180** (2002), 29–48,
[20] O. Diekmann and J. A. P. Heesterbeek, Mathematical epidemiology of infectious diseases, in *Wiley Series in Mathematical and Computational Biology*, John Wiley and Sons, Ltd., Chichester, 2000,
[21] W. E, A proposal on machine learning via dynamical systems, *Math. Sci.*, **5** (2017), 1–11.
[22] G. Giordano, F. Blanchini, R. Bruno, P. Colaneri, A. Filippo, A. Matteo and M. Colaneri, Modelling the COVID-19 epidemic and implementation of population-wide interventions in italy, *Nature Med.*, **26** (2020), 1–6.
[23] D. Greenhalgh, Hopf bifurcation in epidemic models with a latent period and nonpermanent immunity, *Math. Comput. Model.*, **25** (1997), 85–107.
[24] D. Greenhalgh and R. Das, Modeling epidemics with variable contact rates, *Theor. Population Biol.*, **47** (1995), 129–179.
[25] S. Greydanus, M. Dzamba and J. Yosinski, Hamiltonian neural networks, arXiv:1906.01563.
[26] M. R. Hestenes, *Calculus of Variations and Optimal Control Theory*, John Wiley & Sons, Inc., New York-London-Sydney, 1966.
[27] H. W. Hethcote, The mathematics of infectious diseases, *SIAM Rev.*, **42** (2000), 599–653.
[28] S. Hochreiter and J. Schmidhuber, Long short-term memory, *Neural Comput.*, **9** (1997), 1735–1780.
[29] Y. Hosono and B. Ilyas, Traveling waves for a simple diffusive epidemic model, *Math. Models Methods Appl. Sci.*, **5** (1995), 935–966.
[30] E. Hunter, B. Mac Namee and J. Kelleher, An open-data-driven agent-based model to simulate infectious disease outbreaks, *PLOS ONE*, **13** (2018), 1–35.

[31] M. M. Tiberiu Harko Francisco S.N. Lobo, Exact analytical solutions of the susceptible-infected-recovered (SIR) epidemic model and of the SIR model with equal death and birth rates, *Appl. Math. Comput.*, **236** (2014), 184–194.
[32] J. Jang, H. Kwon and J. Lee, Optimal control problem of an SIR reaction-diffusion model with inequality constraints, *Math. Comput. Simul.*, **171** (2020), 136–151.
[33] H. Jo, H. Son, H. J. Hwang and S. Y. Jung, Analysis of COVID-19 spread in South Korea using the SIR model with time-dependent parameters and deep learning, *medRxiv*.
[34] M. Keeling and K. Eames, Networks and epidemic models, *J. Roy. Soc. Interface*, **2** (2005), 295–307.
[35] D. G. Kendall, Mathematical models of the spread of infection, *Math. Comput. Sci. Biol. Med.*, **171** (1965), 213–225.
[36] W. O. Kermack and A. G. McKendrick, A contribution to the mathematical theory of epidemics, *P. Roy. Soc. Lond. A*, **115(772)** (1927), 700–721.
[37] A. Kleczkowski and B. T. Grenfell, Mean-field-type equations for spread of epidemics: The 'small world' model, *Physica A*, **274** (1999), 355–360.
[38] A. Korobeinikov, Global properties of SIR and SEIR epidemic models with multiple parallel infectious stages, *Bull. Math. Biol.*, **71** (2009), 75–83.
[39] I. A. Krylov and F. L. Černous' ko, The method of successive approximations for solving optimal control problems, *Ž. Vyčisl. Mat i Mat. Fiz.*, **2** (1962), 1132–1139.
[40] W. Lee, S. Liu, H. Tembine, W. Li and S. Osher, Controlling propagation of epidemics via mean-field games, arXiv:2006.01249.
[41] M. Y. Li, J. R. Graef, L. Wang and J. Karsai, Global dynamics of a SEIR model with varying total population size, *Math. Biosci.*, **160** (1999), 191–213.
[42] M. Y. Li and J. S. Muldowney, Global stability for the SEIR model in epidemiology, *Math. Biosci.*, **125** (1995), 155–164.
[43] Q. Lin, S. Zhao, D. Gao, Y. Lou, S. Yang, S. Musa, M. Wang, W. Wang, L. Yang and D. He, A conceptual model for the outbreak of coronavirus disease 2019 (COVID-19) in Wuhan, China with individual reaction and governmental action, *Int. J. Infect. Dis.*, **93** (2020), 211–216.
[44] H. Liu and P. Markowich, Selection dynamics for deep neural networks, *J. Differ. Equ.*, **269** (2020), 11540–11574.
[45] W. Liu, H. W. Hethcote and S. A. Levin, Dynamical behavior of epidemiological models with nonlinear incidence rates, *J. Math. Biol.*, **25** (1987), 359–380.
[46] M. Lutter, C. Ritter and J. Peters, Deep lagrangian networks: Using physics as model prior for deep learning, arXiv:1907.04490.
[47] L. Magri and N. A. K. Doan, First-principles machine learning modelling of COVID-19, arXiv:2004.09478.
[48] J. Mena-Lorcat and H. W. Hethcote, Dynamic models of infectious diseases as regulators of population sizes, *J. Math. Biol.*, **30** (1992), 693–716.
[49] R. Parshani, S. Carmi and S. Havlin, Epidemic threshold for the susceptible-infectious-susceptible model on random networks, *Phys. Rev. Lett.*, **104** (2010), 258701.
[50] L. Pontryagin, V. Boltyanskii, R. Gamkrelidze and E. Mishchenko, *The Mathematical Theory of Optimal Processes*, CRC Press, 1962.
[51] M. Raissi, P. Perdikaris and G. E. Karniadakis, Physics-informed neural networks: a deep learning framework for solving forward and inverse problems involving nonlinear partial differential equations, *J. Comput. Phys.*, **378** (2019), 686–707.
[52] T. C. Reluga and A. P. Galvani, A general approach for population games with application to vaccination, *Math. Biosci.*, **230** (2011), 67–78.
[53] R. T. Rockafellar, Monotone operators and the proximal point algorithm, *SIAM J. Control Optim.*, **14** (1976), 877–898.
[54] W. H. Schmidt, Numerical methods for optimal control problems with ODE or integral equations, in *Large-Scale Scientific Computing*, vol. 3743 of Lecture Notes in Comput. Sci., Springer, Berlin, 2006,
[55] R. Sun, Global stability of the endemic equilibrium of multigroup SIR models with nonlinear incidence, *Comput. Math. Appl.*, **60** (2010), 2286–2291.
[56] H. R. Thieme, Epidemic and demographic interaction in the spread of potentially fatal diseases in growing populations, *Math. Biosci.*, **111** (1992), 99–130.
[57] D. J. Watts, Small worlds, in *Princeton Studies in Complexity*, Princeton University Press, Princeton, NJ, 1999,

[58] S. H. White, A. M. del Rey and G. R. Sánchez, Modeling epidemics using cellular automata, *Appl. Math. Comput.*, **186** (2007), 193–202.

Received December 2020; revised April 2021.